EasyChair Preprint

№ 1716

Comparison of basic droop control with linear and nonlinear internal control of boost converters feeding resistive load

Sonia Moussa, Manel Jebali-Ben Ghorbal and
Ilhem Slama-Belkhodja

October 19, 2019

IMAT3E'19

International Meeting on Advanced Technologies in Energy and Electrical Engineering

28-29 Nov. 2019 Tunis, Tunisia

Comparison of basic droop control with linear and nonlinear internal control of boost converters feeding resistive load

Sonia MOUSSA
Université de Tunis El Manar, Ecole Nationale d'Ingénieurs de Tunis, LR11ES15 Laboratoire des Systèmes Electriques, 1002,
Tunis, Tunisia
sonia.moussa@enit.utm.tn

Manel JEBALI-BEN GHORBAL
Université de Tunis El Manar, Ecole Nationale d'Ingénieurs de Tunis, LR11ES15 Laboratoire des Systèmes Electriques, 1002,
Tunis, Tunisia
manel.jebalibenghorbal@enit.utm.tn

Ilhem SLAMA-BELKHODJA
Université de Tunis El Manar, Ecole Nationale d'Ingénieurs de Tunis, LR11ES15 Laboratoire des Systèmes Electriques, 1002,
Tunis, Tunisia
ilhem.slamabelkhodja@enit.utm.tn

***Abstract*— Over the past few decades, DC microgrids as off-grid solution for rural areas electrification have been trendy, thanks to their advantages over AC microgrids in terms of efficiency, size and cost. One of the major concerns on DC microgrid implementation is the parallel operating of the distributed generators. Hence, this paper addresses the application of basic droop control considering parallel operating of two distributed generators in a standalone residential DC microgrid. A comparison of performance when considering a linear control and nonlinear control of the internal variables of the boost converter is performed. Simulation results are presented using PSIM.**

Keywords—boost converter, droop control, current load sharing.

I. INTRODUCTION

The proliferation on the market of small-scale renewable energy sources that generate electricity in DC form has more and more facilitate the development of off-grid solution for non-electrified rural region in the world. In this sense, numerous DC home appliances are available on the market [1], greatly promoting residences with DC distribution system [2]–[5]. Coupled to this, the growing trend toward the use of all-electric vehicles will make the battery storage system more affordable with a better storage capacity. This will greatly contribute to the adoption of LVDC microgrid for residential application as presented in Fig. 1. This field is actually gathering the intention of many researchers, covering the branch of standardization [6], [7], control strategy [8], [9], power flow management [10], [11], operation stability, storage technologies and control [12], [13], renewable source efficiency[14].

Regarding the control strategy, the first layer of hierarchical control concerns the current load sharing among the paralleled converters [8]. Often, error load sharing occurs when there is a mismatch of voltage values provided by the sources at the bus level. If the output voltage of each converter is well regulated, then this mismatch comes from the difference in cable impedance connecting the converters to the DC bus [15].

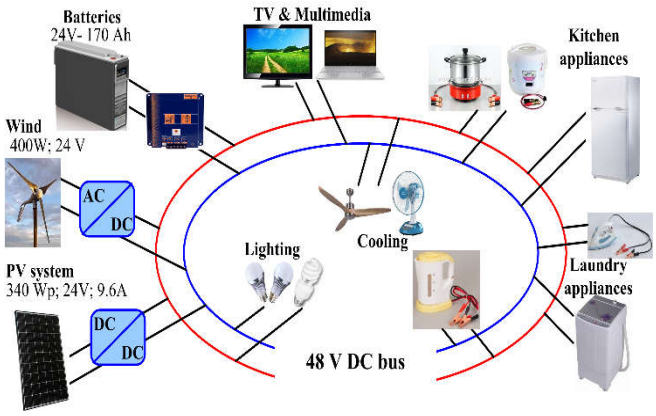

Fig. 1. Residential DC microgrid

To overcome the error in current load sharing, some types of controls, such as active load sharing and droop control have been proposed in the literature. If the active load sharing method presents the advantages of being simple to implement with a good performance, its major drawbacks reside in the need of a large bandwidth communication link and its low flexibility and modularity. In fact, a higher bandwidth communication link is needed with the increasing number of distributed generators present in the microgrid. Droop control, on the other hand, presents a poorer current load sharing capacity compared to the active load sharing method, but it does not need a communication link for its implementation and the modularity of the system elements is not affected in the case of an add or removal of distributed generators. Eventually, a low-bandwidth communication link is enough in case of a droop control with voltage restoration.

Hence, in this paper, droop control is chosen as load sharing method, the purpose being a performance comparison when the internal variable of the converter is controlled using linear and nonlinear controllers.

The paper is structured as follows: a presentation of the studied system, detailing the power stage modeling, the controller synthesis, and droop control application, is presented in section 2. Section 3 discusses the simulation results while section 4 gives a conclusion of the paper.

II. STUDIED SYSTEM PRESENTATION

A. Power stage model

As the interest is laid on the parallel operating of distributed generators, we consider the system presented in Fig. 2. The studied system is composed of two distributed generators with their interfacing converter and a resistive load. Non-isolated boost converter is taken as interfacing converter. The DC bus level chosen for application is 48 V, while the input voltages of the sources are inferior to this value. This choice of voltage level has been discussed in [1]. The resistances rc1 and rc2 represent the cable resistance connecting each converter to the bus.

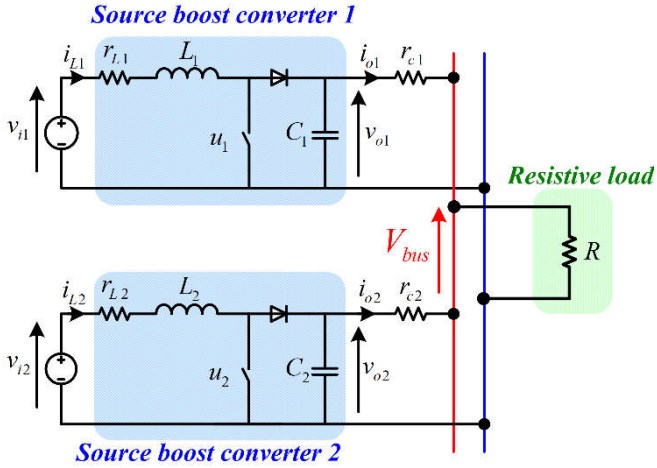

Fig. 2. Case-study system

The power loss in the inductor of the converters is taken into account since it presents a great impact on the converter output voltage. This loss is portrayed by the resistances r_{L1} and r_{L2}. The large signal average model system of equations governing each converter is given by (1), where the subscript k is related to each converter.

$$\begin{bmatrix} \frac{di_{Lk}}{dt} \\ \frac{dv_{ok}}{dt} \end{bmatrix} = \begin{bmatrix} -\frac{r_{Lk}}{L_k} & -\frac{1-d_k}{L_k} \\ \frac{1-d_k}{C_k} & -\frac{1}{R_k C_k} \end{bmatrix} \begin{bmatrix} i_{Lk} \\ v_{ok} \end{bmatrix} + \begin{bmatrix} \frac{1}{L_k} \\ 0 \end{bmatrix} v_{ik} \quad (1)$$

In (1), d_k represents the duty cycle associated with the k^{th} converter and R_k represents the load resistance for a given power consumed P by the converter and is expressed by

$$R_k = \frac{v_{ok}^2}{P_{ok}} \quad (2)$$

Since linear controller will be considered later, the small signal average model describing the boost converter is given by (3)

$$\begin{bmatrix} \frac{d\widetilde{i_{Lk}}}{dt} \\ \frac{d\widetilde{v_{ok}}}{dt} \end{bmatrix} = \begin{bmatrix} -\frac{r_{Lk}}{L_k} & -\frac{1-D_k}{L_k} \\ \frac{1-D_k}{C_k} & -\frac{1}{R_k C_k} \end{bmatrix} \begin{bmatrix} \widetilde{i_{Lk}} \\ \widetilde{v_{ok}} \end{bmatrix} + \begin{bmatrix} \frac{V_{ok}}{L_k} \\ -\frac{I_{Lk}}{C_k} \end{bmatrix} \widetilde{d_k} + \begin{bmatrix} \frac{1}{L_k} \\ 0 \end{bmatrix} \widetilde{v_{ik}} \quad (3)$$

This small signal average model is obtained by a linearization of (2) around an operating point of the converter. Each variable of (2) is defined as a sum of an average value and a small variation around this average value, as expressed in (4).

$$\begin{aligned} i_{Lk} &= I_{Lk} + \widetilde{i_{Lk}} \\ v_{ok} &= V_{ok} + \widetilde{v_{ok}} \\ d_k &= D_k + \widetilde{d_k} \\ v_{ik} &= V_{ik} + \widetilde{v_{ik}} \end{aligned} \quad (4)$$

Equations governing the power stage being defined, the synthesis of each controller type is then detailed in the following subsection B.

B. Controller synthesis

For the controller synthesis of the converter intern variable, Proportional-Integral regulator is first considered

1) Linear PI controller synthesis

The PI controller synthesis goes through the description of the transfer function of the variable to be controlled. Since in our case, the inductor current and the output voltage of the converter are both controlled, a cascaded control loop is adopted. The block diagram illustration the control is presented in Fig. 3.

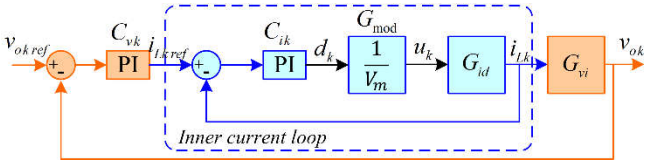

Fig. 3. Linear control block diagram

Since cascaded loop is used, the inner current loop dynamic must be fast compared to the outer voltage loop.

By using the Laplace transform of (3), and by considering $\widetilde{v_{ik}}$ as a perturbation, the control-to-current transfer function G_{id} is expressed by (5).

$$G_{id}(s) = \frac{\widetilde{i_{Lk}}}{\widetilde{d_k}} = \frac{V_{ok}}{sL_k + r_{Lk}} \quad (5)$$

This expression is obtained while neglecting the term in $\widetilde{v_{ok}}$ of the Laplace transform of (3), since the dynamic of the outer loop is considered slow compared to inner loop one.

Current-to-output voltage transfer function case is obtained by assuming the inductor current equal to its reference after a transient in the current loop. Since the inner loop is much faster than the outer loop, the perturbation in the duty cycle can be neglected. Therefore, the current-to-output voltage transfer function expression is given by (6).

$$G_{vi}(s)=\frac{\widetilde{v_{ok}}}{\widetilde{i_{Lk}}}=\frac{(1-D_k)}{sC_k+\dfrac{1}{R_k}} \tag{6}$$

The expression of the PI controller associated to each loop is then given by (7) and (9) respectively for the current and voltage controllers.

$$C_{ik}(s)=K_{pik}+\frac{K_{iik}}{s} \tag{7}$$

$$C_{vk}(s)=K_{pvk}+\frac{K_{ivk}}{s} \tag{8}$$

As the voltage and current loop transfer functions are 1st order ones, the controller synthesis is done by pole compensation.

2) Nonlinear controller synthesis

Similar to the synthesis of the linear controller, a cascaded controller as in [16] is also adopted. The control of the inductor current, the inner loop control, is realized by sliding mode control while the outer loop voltage control is done by flatness-based control. The schematic block diagram depicting the control is presented in Fig. 4.

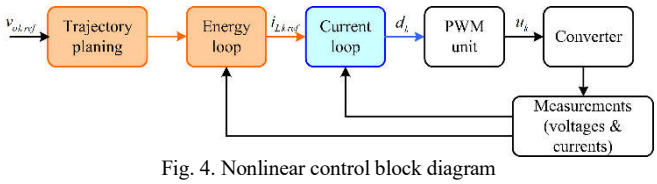

Fig. 4. Nonlinear control block diagram

The sliding surface S_k of the sliding mode controller and the condition on its derivative is given in (9).

$$\begin{aligned} S_k &= i_{Lk}-i_{Lkref}+K_{ik}\int\left(i_{Lk}-i_{Lkref}\right)d\tau \\ \dot{S}_k &= -\lambda_k S_k \end{aligned} \tag{9}$$

From (9), one can draw the duty cycle's expression that is given by (10).

$$\begin{aligned} D_k &= \frac{1}{V_{ok}}\left(a_k+b_k\right) \\ a_k &= V_{ok}+r_{Lk}i_{Lk}-V_{ik} \\ b_k &= L_k\left[\left(K_{ik}+\lambda_k\right)\left(i_{Lkref}-i_{Lk}\right)+K_{ik}\lambda_k\int\left(i_{Lkref}-i_{Lk}\right)\right] \end{aligned} \tag{10}$$

For the flatness-based control of the outer loop, the energy of the output voltage capacitor is taken as flat output candidate y. its expression is given by (11):

$$y=\frac{1}{2}C_k{v_{ok}}^2 \tag{11}$$

A power balance of the converter is then realized in order to establish the relation between the control variable i_{Lk} and the flat output candidate y. we assume that the power induced by the variation of the magnetic energy is negligible and the current loop dynamic is much faster than the outer loop.

$$\dot{y}=P_{in}-r_{Lk}{i_{Lk}}^2-P_{ok}=P_{in}-r_{Lk}\left(\frac{P_{in}}{v_{ik}}\right)^2-P_{ok} \tag{12}$$

The current control is then obtained by resolving (12) and is expressed by (13).

$$i_{Lk}=\frac{P_{in}}{V_{ik}}=\frac{2P_{i\max}}{V_{ik}}\left(1-\sqrt{1-\frac{\dot{y}+P_{ok}}{P_{i\max}}}\right) \tag{13}$$

With $P_{i\max}=\dfrac{{V_{ik}}^2}{4r_{Lk}}$: maximum transmissible power

$P_{ok}=v_{ok}i_{ok}$: output power

The control law adopted for the energy of the output capacitor is given by

$$\left(\dot{y}-\dot{y}_{ref}\right)+K_{py}\left(y-y_{ref}\right)+K_{iy}\int\left(y-y_{ref}\right)d\tau=0 \tag{14}$$

Thus, the expression of $\dot{y}$ in (13) is deduced from (14) and expressed as follows:

$$\dot{y}=\dot{y}_{ref}+K_{py}\left(y_{ref}-y\right)+K_{iy}\int\left(y_{ref}-y\right) \tag{15}$$

The nonlinear controller block diagram is thus illustrated in Fig. 5.

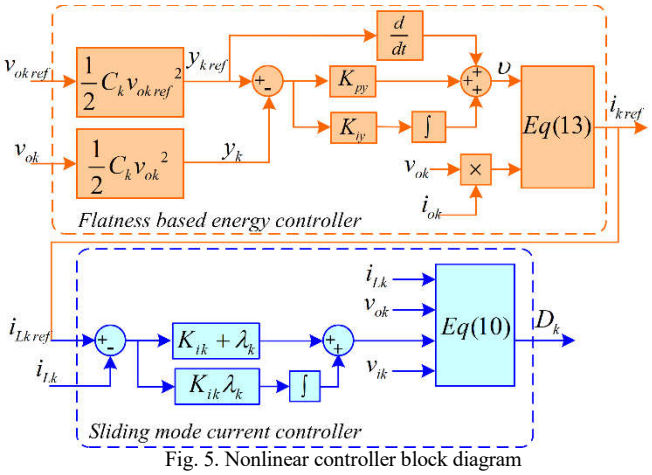

Fig. 5. Nonlinear controller block diagram

C. Droop control with voltage restoration

In order to simplify the comprehension of the droop control principle, let us consider the output voltage v_{ok} of each converter well-regulated and assimilated to a voltage source as shown in Fig. 6. The droop control consists in emulating virtual impedance R_{Dk} in each branch containing a source, so that having the same voltage value on the bus. This feat is performed by using an outer loop with a droop gain, that is subtracted to the control loop of the converter.

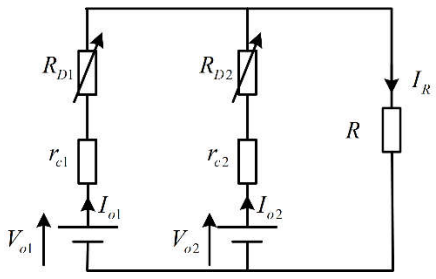

Fig. 6. Droop control principle

The reference $V_{o\,kref}$ of the output voltage of the converter then becomes as expressed in (16), $V_{ref\,k}$ being the fixed value

of the desired bus voltage, R_{Dk} the virtual droop resistance and i_{ok} the output current of the converter.

$$V_{ok\,ref} = V_{ref\,k} - R_{Dk}\, i_{ok} \tag{16}$$

Considering the maximum output voltage deviation ε_v and the maximum output current $I_{ok\,max}$ of the converter, the virtual resistance R_{Dk} is calculated as in (17).

$$R_{Dk} = \frac{\varepsilon_v}{I_{ok\,\max}} \tag{17}$$

From (16), one can deduce that the output voltage of the converter will be lower than the desired reference, due to the virtual resistance. Hence, another outer loop that allows restoring the bus voltage, according to the drop occasioned by the virtual resistance, is added to the overall control. Finally, the output voltage reference of the converter is given by (18), where δv_{ok} represents the processed voltage deviation.

$$V_{ok\,ref} = V_{ref\,k} - R_{Dk}\, i_{ok} + \delta v_{ok} \tag{18}$$

The processed voltage deviation δv_{ok} results from the compensation through PI regulator of the sensed bus voltage V_{bus} and the desired bus voltage $V_{bus\,ref}$.

The outer loop control to be added to the control of the internal variable of the converter is then depicted in Fig. 7.

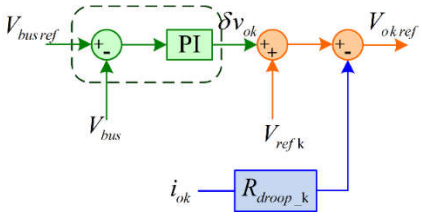

Fig. 7. Droop control with voltage restoration

III. Simulations and Discussions

In order to compare the performance of the droop control combined with the two types of control for the internal variable of the converters, two scenarios will be considered. For both scenarios, a resistance of 3.84 Ω is taken as load, that corresponds to a consumed power of 600 W. The cable resistance linking the first converter to the bus is the double of the one linking the second converter. And both converters have the same characteristic.

In the first scenario (*scenario 1*), the input voltages of both converters are the same while the second scenario (*scenario 2*) is the case where the input voltages of the converters are different.

For each scenario, the evolution of the voltage and current with and without droop control is shown.

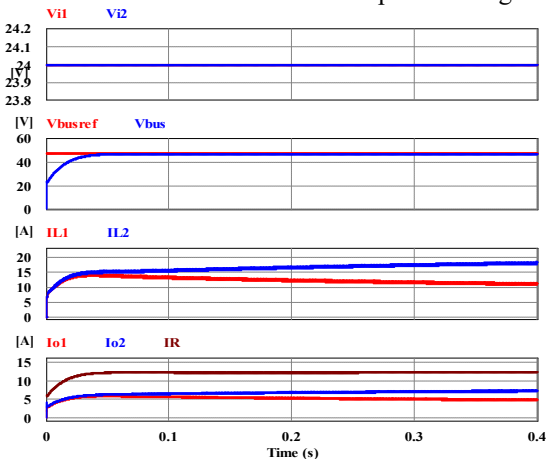

(a) Without droop control

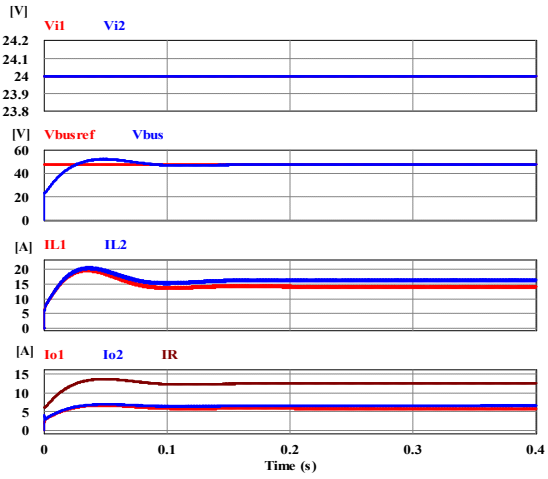

(b) With droop control

Fig. 8. Scenario 1 with PI controllers

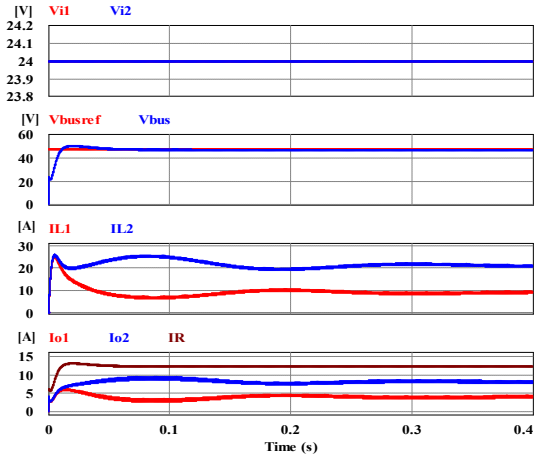

(a) Without droop control

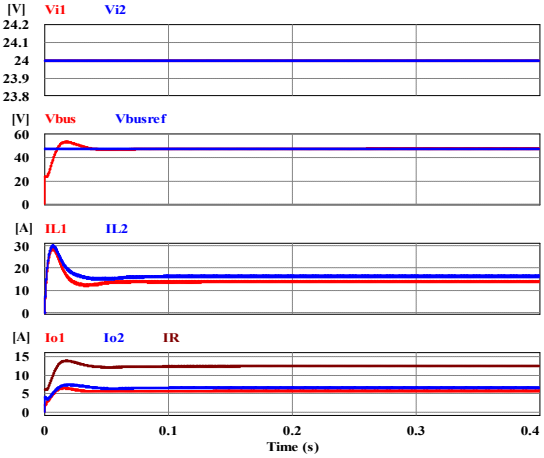

(b) With droop control

Fig. 9. Scenario 1 with nonlinear controllers

Fig. 8 and Fig. 9 show the simulation results of the first scenario when adopting linear and nonlinear controllers respectively, while Fig. 10 highlights the behavior of the droop controlled-system in steady-state.

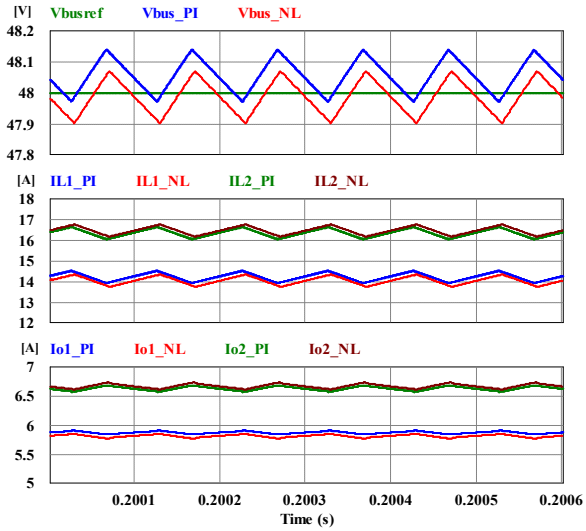

Fig. 10. Zoom scenario 1 for droop control in steady-state

As can be seen in Fig. 8(a) and Fig. 9(a), despite the converters having the same characteristics and the same operating point the one connected to the bus through a lower cable resistance, here the *converter 2*, have to produce more current to the load. The error in current load sharing is worse for the nonlinear controlled-system compared to the one linear-controlled.

However, after applying the droop control as presented in Fig. 8(b) and Fig. 9(b), the error load sharing is minimized. The transient of the nonlinear-controlled system is faster than the one of the linear-controlled one, but it has a high inrush current.

One the other hand, during the steady-state operation as shown in Fig. 10, the current load sharing is almost identical whether the system is internally controlled in a linear or nonlinear way. Nonetheless, the bus regulation of the nonlinear-controlled system is better.

The second scenario simulation results are given in Fig. 11 and Fig. 12, respectively, when adopting linear and nonlinear controllers. Likewise in the first scenario, the zoom operation in steady-state while droop control is applied is presented in Fig. 13.

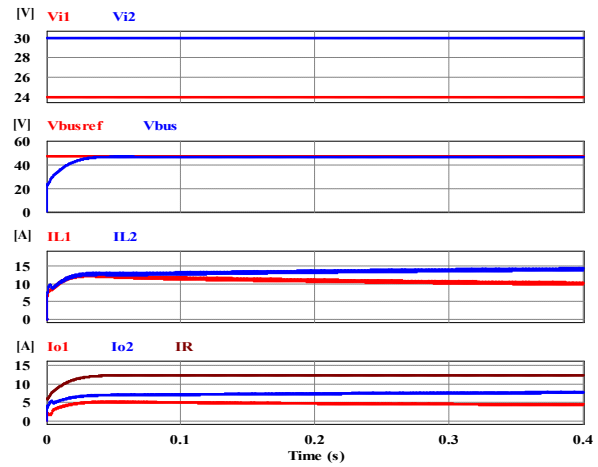

(a) Without droop control

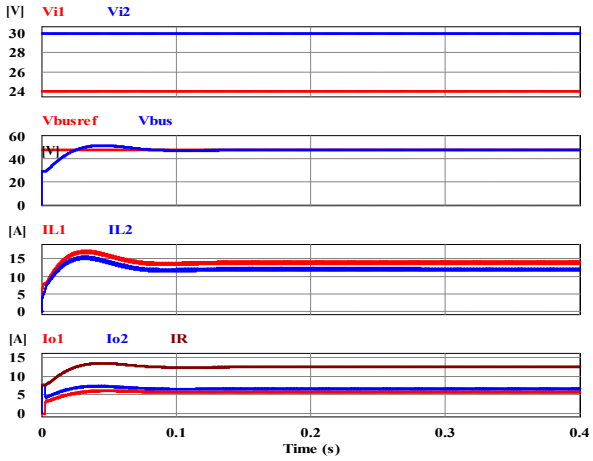

(b) With droop control

Fig. 11. Scenario 2 with PI controllers

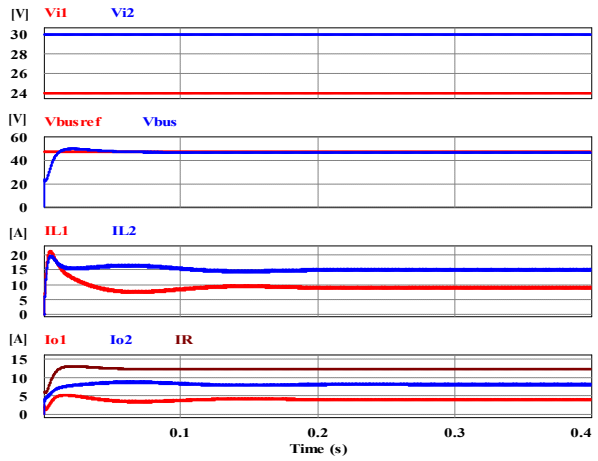

(a) Without droop control

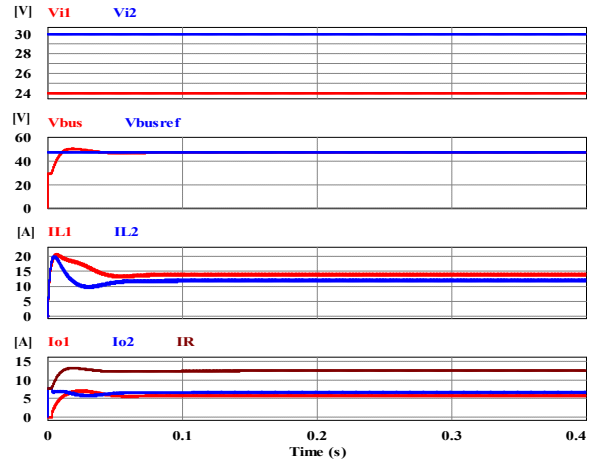

(b) With droop control

Fig. 12. Scenario 2 with nonlinear controllers

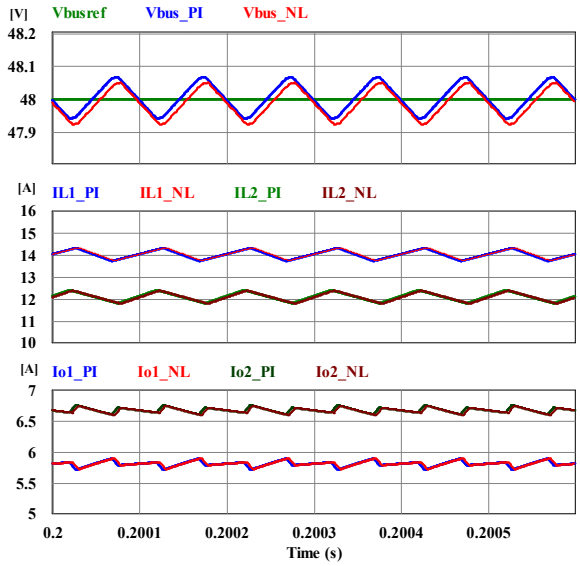

Fig. 13. Zoom scenario 2 for droop control in steady-state

Despite the input voltage of *converter 2* is greater than the one of *converter 1*, the error load sharing remains, as can be seen in Fig. 11(a) and Fig. 12(a). The converter with the lower cable resistance is still overworked. The application of droop control minimizes the error load sharing among the converters as shown in Fig. 11(b) and Fig. 12(b). The system controlled non-linearly is still faster with high inrush current. However, the zoom in steady-state operation presented in Fig. 13 shows an almost identical current sharing and voltage regulation for both linear and nonlinear controlled system.

IV. Conclusion

In this paper, the parallel operation of two boost converters feeding a resistive load is investigated and compared considering a linear and nonlinear control of the internal variables of these converters. The cable resistances linking the converters to the DC bus are taken different and it has been shown that a non-negligible error load sharing occurs among the converters, whether the input voltages of the converters are identical or different. The application of droop control on the system gives almost identical results in steady-state operation, though the nonlinear-controlled system is faster with a higher inrush current compared to the linear-controlled one.

In perspective, the application of droop control with the same system while considering a constant power load type will be investigated later.

Acknowledgment

This work was supported by the Tunisian Ministry of High Education and Research under Grant LSE-ENIT-LR 11ES15 and funded in part by NAS and USAID under the USAID Prime Award Number AID-OAA-A-11-00012. Any opinions, findings, conclusions, or recommendations expressed in this article are those of the authors alone, and do not necessarily reflect the views of USAID or NAS.

References

[1] S. Moussa, M. Jebali-Ben Ghorbal, and I. Slama-Belkhodja, “Bus voltage level choice for standalone residential DC nanogrid,” *Sustain. Cities Soc.*, vol. 46, p. 101431, Apr. 2019.

[2] T. Taufik and M. Muscarella, “Development of DC house prototypes as demonstration sites for an alternate solution to rural electrification,” in *2016 6th International Annual Engineering Seminar (InAES)*, 2016, pp. 262–265.

[3] T. Castillo-Calzadilla, A. M. Macarulla, O. Kamara-Esteban, and C. E. Borges, “Analysis and assessment of an off-grid services building through the usage of a DC photovoltaic microgrid,” *Sustain. Cities Soc.*, vol. 38, pp. 405–419, Apr. 2018.

[4] S. Golshannavaz and V. Mortezapour, “A generalized droop control approach for islanded DC microgrids hosting parallel-connected DERs,” *Sustain. Cities Soc.*, vol. 36, pp. 237–245, Jan. 2018.

[5] P. Ghalebani and M. Niasati, “A distributed control strategy based on droop control and low-bandwidth communication in DC microgrids with increased accuracy of load sharing,” *Sustain. Cities Soc.*, vol. 40, pp. 155–164, Jul. 2018.

[6] J. Decuir and P. Michael, “Draft IEEE standard for DC microgrids for rural and remote electricity access applications,” in *2017 IEEE Conference on Technologies for Sustainability (SusTech)*, 2017, pp. 1–5.

[7] T. Kaipia *et al.*, “Survey of market prospects and standardisation development needs of LVDC technology,” *CIRED - Open Access Proc. J.*, vol. 2017, no. 1, pp. 454–458, 2017.

[8] S. Augustine, M. K. Mishra, and N. Lakshminarasamma, “Adaptive droop control strategy for load sharing and circulating current minimization in low-voltage standalone DC microgrid,” *Sustain. Energy IEEE Trans. On*, vol. 6, no. 1, pp. 132–141, 2015.

[9] O. Cornea, G. Andreescu, N. Muntean, and D. Hulea, “Bidirectional Power Flow Control in a DC Microgrid Through a Switched-Capacitor Cell Hybrid DC–DC Converter,” *IEEE Trans. Ind. Electron.*, vol. 64, no. 4, pp. 3012–3022, Apr. 2017.

[10] X. Y. Chen and J. X. Jin, “Energy Efficiency Analysis and Energy Management of a Superconducting LVDC Network,” *IEEE Trans. Appl. Supercond.*, vol. 26, no. 7, pp. 1–5, Oct. 2016.

[11] E. Rodriguez-Diaz, E. J. Palacios-Garcia, A. Anvari-Moghaddam, J. C. Vasquez, and J. M. Guerrero, “Real-time Energy Management System for a hybrid AC/DC residential microgrid,” in *2017 IEEE Second International Conference on DC Microgrids (ICDCM)*, 2017, pp. 256–261.

[12] W. W. Weaver, R. D. Robinett, G. G. Parker, and D. G. Wilson, “Energy storage requirements of dc microgrids with high penetration renewables under droop control,” *Int. J. Electr. Power Energy Syst.*, vol. 68, pp. 203–209, 2015.

[13] C. Mahjoubi, J.-C. Olivier, S. Skander-mustapha, M. Machmoum, and I. Slama-belkhodja, “An improved thermal control of open cathode proton exchange membrane fuel cell,” *Int. J. Hydrog. Energy*, vol. 44, no. 22, pp. 11332–11345, Apr. 2019.

[14] A. Triki-Lahiani, A. Bennani-Ben Abdelghani, and I. Slama-Belkhodja, “Partial shading effect investigation on PV performance indicators,” in *2018 9th International Renewable Energy Congress (IREC)*, 2018, pp. 1–6.

[15] S. Moussa, M. Jebali-Ben Ghorbal, and I. Slama-Belkhodja, “DC Load Modelling and Droop Control Analysis for Autonomous Residential DC Microgrid,” presented at the ELECTRIMACS 2017, Toulouse - FRANCE, 2017, pp. 1–6.

[16] R. Gavagsaz-Ghoachani, L. M. Saublet, J. P. Martin, B. Nahid-Mobarakeh, and S. Pierfederici, “Stability Analysis and Active Stabilization of DC Power Systems for Electrified Transportation Systems, Taking into Account the Load Dynamics,” *IEEE Trans. Transp. Electrification*, vol. 3, no. 1, pp. 3–12, Mar. 2017.